IJCA

Indonesian Journal of Chemical Analysis

Homepage: https://journal.uii.ac.id/IJCA

Synthesis of Biochar-Like Graphene Nanosheets (BLG) from Candlenut Shells with Integrated Conductive and Antibacterial Functionalities

Friscilla Romiduk Samosir[a,c], Mohd Fakharul Zaman Raja Yahya[d], Rikson Siburian [a,b,c,*]

[a] Department of Chemistry, Faculty of Mathematics and Natural Sciences, Universitas Sumatera Utara, Medan 20155, Indonesia
[b] Carbon and Frankincense Research Center, Universitas Sumatera Utara, Medan 20155, Indonesia
[c] Department of Postgraduate of Chemistry, Faculty of Mathematics and Natural Sciences, Universitas Sumatera Utara, Medan 20155, Indonesia
[d] Faculty of Applied Sciences, Universiti Teknologi MARA (UiTM), 40450 Shah Alam, Selangor, Malaysia
*corresponding author: rikson@usu.ac.id
DOI: 10.20885/ijca.vol8.iss2.art7

GRAPHICAL ABSTRACT

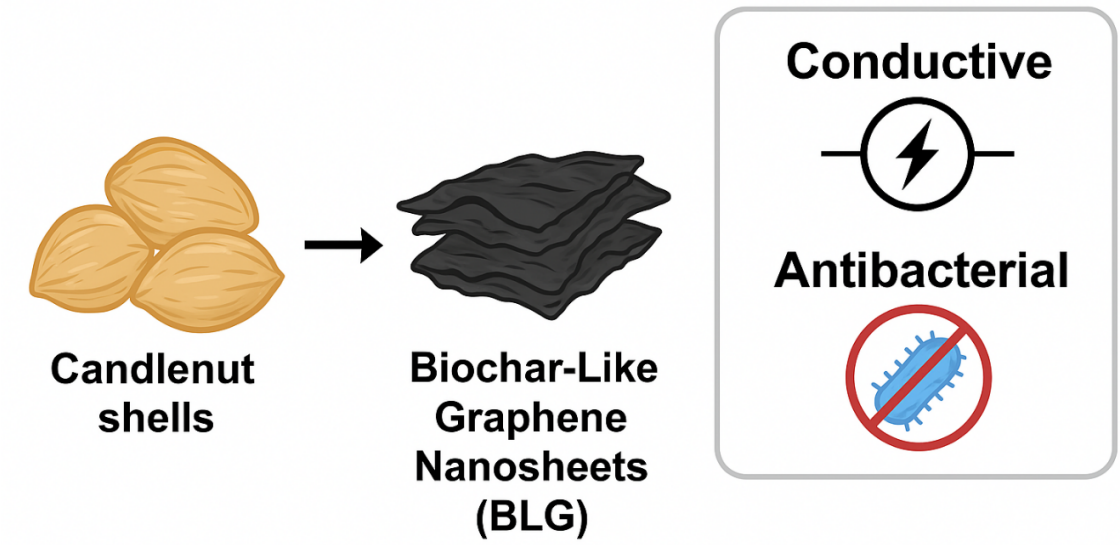

ARTICLE INFO

Received : 20 August 2025
Revised : 16 September 2025
Published : 29 September 2025
Keywords : Biomass-derived graphene nanosheets, Candlenut shell, Electrical conductivity, Antibacterial activity, Salmonella typhimurium

ABSTRACT

Graphene's exceptional electrical, mechanical, and chemical properties have enabled breakthroughs in electronics, energy storage, and biomedicine, yet large-scale, low-cost, and sustainable production methods remain elusive. Here, we report a facile, scalable route to synthesize Biochar-Like Graphene Nanosheets (BLG) from candlenut shell biomass using activated carbon as a dual-function reducing agent and combustion inhibitor in a modified muffle furnace pyrolysis system. Structural analysis by X-ray diffraction and Fourier-transform infrared spectroscopy confirms the formation of defect-rich, low-oxygen sp^2 carbon networks, while scanning electron microscopy reveals wrinkled layered morphologies that promote electrolyte accessibility. Electrical measurements demonstrate a voltage-dependent conductivity, reaching 368.67 $\mu S \cdot cm^{-2}$ at 1.5 V, alongside stable power density (6.72 $W \cdot kg^{-1}$) and high energy density (403.2 $Wh \cdot kg^{-1}$), indicative of excellent charge transport and storage capabilities. Remarkably, BLG exhibits potent antibacterial activity against Salmonella typhimurium with a 10.76 ± 0.23 mm

inhibition zone and positive MIC and MBC responses, attributed to synergistic membrane disruption, reactive oxygen species generation, and electron transfer effects. This biomass-to-graphene strategy offers a sustainable, multifunctional nanomaterial platform for next-generation energy, environmental, and biomedical technologies.

1. INTRODUCTION

Graphene is the thinnest two-dimensional material of carbon atoms arranged in a hexagonal lattice. It exhibits exceptional thermal, mechanical, and electrical conductivity properties, coupled with a high specific surface area of up to 2630 $m^2.g^{-1}$, low sheet resistance, excellent mechanical strength, and ultralight weight. These unique characteristics make graphene highly promising for various applications, including electronics, energy storage, and biomedical systems [1]. Despite its outstanding potential, graphene synthesis still faces significant challenges, particularly in large-scale production, quality control, and cost efficiency [2].

To address these limitations, various synthesis strategies have been explored, such as chemical vapor deposition (CVD), epitaxial growth, arc discharge, modified Hummers' method, liquid-phase exfoliation, mechanical exfoliation, supercritical fluid techniques, sonication, and carbon nanotube unzipping. However, none of these methods can be considered ideal for industrial-scale implementation. Graphene can be derived from different carbon precursors, including graphite, coal, methane, biomass, and other carbon-rich sources [3, 4]. Among these, biomass has emerged as an attractive alternative owing to its low cost, abundance, and sustainability. Recent studies have demonstrated the feasibility of producing graphene nanosheets from biomass for various applications, including primary batteries [5].

Candlenut shell, an agricultural byproduct, is particularly promising due to its high carbon content, primarily composed of lignin (54.6%) and cellulose (49.2%) [6, 7]. Previous work reported the synthesis of Biochar-like graphene nano sheets (BLG) using a one-step pyrolysis approach, resulting in multilayer graphene sheets [8]. However, this method relies on advanced reactor systems and is limited by reactor size, hindering scalability.

The present study aims to develop a simplified and scalable synthesis method for BLG derived from candlenut shell biomass. Activated carbon was employed as both a reducing agent and a combustion inhibitor during pyrolysis, facilitating oxygen removal while suppressing unwanted oxidation. The resulting graphene material is expected to exhibit nano-layered morphology with properties suitable for applications as a conductive material and antibacterial agent.

2. EXPERIMENTAL METHODS

The candlenut shell waste was obtained from community-owned plantations in Sidikalang District, Dairi Regency, North Sumatra. This experiment was carried out using a modified pyrolysis method approach.

2.1. Synthesis of BLG

The candlenut shell was cleaned from ash using a brush and directly mixed with activated carbon powder in a ratio of charcoal to activated carbon (1:1) [9], then pyrolyzed in a furnace at 600 °C for 4 hours in an air atmosphere. The heating rate was set to 10 °C·min^{-1}, reaching 600 °C. Afterward, the candlenut shell charcoal chips were separated from the activated carbon, washed with distilled water, and dried in an oven at 105 °C for 4 hours. Subsequently, the BLG was ground using a grinder and sieved with a 200-mesh sieve.

2.2. Sample Characterization

The sample was characterized using X-ray Diffraction (XRD, Rigaku Corporation, Japan), Scanning Electron Microscopy (SEM, JEOL 2100F, Japan), and Fourier Transform Infrared Spectroscopy (FTIR, Agilent Cary 630, United States).

2.3. Conductivity Measurement

A total of 300 mg of BLG powder was packed into a fused quartz tube with an internal diameter of 0.3 cm and a length of 2.0 cm. Alligator clip cables were attached to both ends of the tube and connected to a multimeter's negative and positive terminals, integrated with a regulated DC power supply. The electrical conductivity (EC) of the BLG was measured by applying voltages of 0.5, 1.0, and 1.5 V, while the corresponding current (mA) readings were recorded from the multimeter display as shown in Figure 1 [9].

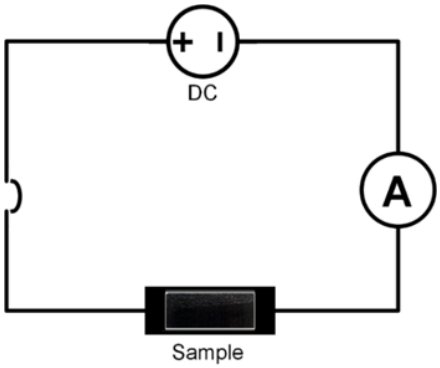

Figure 1. Electrical circuit model for conductivity measurements.

The energy density (E) and power density (P) were estimated from the electrical conductivity measurements using the following equations:

$$E = (V \times I \times t) / m \quad (1)$$

$$P = (V \times I) / m \quad (2)$$

V is the applied voltage, I is the measured current, t is the measurement time, and m is the mass of the BLG sample (300 mg). These values indicate the charge storage capability of BLG under the applied conditions. However, they are not directly equivalent to conventional electrochemical testing methods such as cyclic voltammetry or galvanostatic charge–discharge in a whole cell.

2.4. Antibacterial analysis

The antibacterial activity of candlenut shell extract and biochar-like graphene-based material (BLG) against *Salmonella typhimurium* was evaluated using the agar well diffusion method, determination of Minimum Inhibitory Concentration (MIC), and Minimum Bactericidal Concentration (MBC). A bacterial suspension was prepared by diluting a pure colony in 0.9% physiological NaCl solution until turbidity reached that of a 0.5 McFarland standard. Mueller–Hinton Agar (MHA) plates were prepared for the agar well diffusion assay, and wells with a 6 mm diameter were created using a sterile cork borer. Each well was filled with 0.1 mL of the sample solution at a concentration of 300 mg/mL. The plates were incubated at 37 °C for 24 h. Antibacterial activity was assessed by measuring the inhibition zone diameter around each well. MIC determination was performed by adding 100 µL of bacterial suspension and 100 µL of the sample solution (1 mg/mL) into a sterile 96-well microtiter plate, followed by incubation at 37 °C for 24 h. The MIC was defined as the lowest concentration at which no visible bacterial growth was observed. MBC determination was carried out by transferring 50 µL from MIC-negative wells onto Brain Heart Infusion (BHI) agar plates, followed by incubation at 37 °C for 24 h. The MBC was the lowest concentration capable of killing ≥99.9% of the bacterial population [10].

3. RESULTS AND DISCUSSIONS

Biochar-like graphene nanosheets (BLG) were synthesized through a one-step pyrolysis process and thoroughly characterized by XRD, FTIR, and SEM to elucidate their structural and functional properties. Subsequently, the material was assessed for antibacterial efficacy and evaluated for its electrical performance.

3.1. XRD Study

X-ray diffraction (XRD) analysis was carried out using an XRD instrument manufactured by Rigaku Corporation (Japan). The instrument operated at 18 kW with a tube voltage of 40 kV and a current of 100 mA, employing a 10 mm × 10 mm beam size and Cu Kα radiation (λ = 1.5406 Å) with a graphite monochromator. The diffraction patterns were recorded over a 2θ range of 10°–90° with a step size of 2°. The use of candlenut shells as a carbon precursor offers a sustainable and cost-effective alternative to conventional graphene synthesis routes. Unlike harsh chemical oxidation or chemical vapor deposition, this approach leverages a biomass-derived source and a one-step pyrolysis process to enhance structural integrity. The incorporation of activated carbon during pyrolysis plays a dual role: it suppresses unwanted combustion, ensuring a controlled carbonization environment, and promotes in-situ reduction of oxygen functionalities, which is critical for generating graphitic domains at relatively low temperatures [6].

The interlayer spacing (d) was determined using XRD data based on Bragg's law, which describes the condition for constructive interference of X-rays reflected by crystal planes:

$$2\,d\sin\theta = n\lambda \quad (1)$$

where d is the interplanar spacing, λ is the X-ray wavelength, θ is the diffraction angle, and n is an integer representing the order of reflection.

The average crystallite size (D) was calculated using the Scherrer equation:

$$D = \frac{K\lambda}{\beta\cos\theta} \quad (2)$$

where K is the shape factor (0.9), λ is the X-ray wavelength (1.5406 Å for Cu Kα radiation), β is the full width at half maximum (FWHM) in radians, and θ is the Bragg angle.

Crystallinity was evaluated by deconvolution of the XRD pattern into crystalline and amorphous contributions to assess the degree of structural ordering. The crystallinity index (CI) was computed as:

$$\text{Crytallinity}\ (\%) = \frac{Total\ crystalin\ area}{Total\ area} \quad (3)$$

A higher crystalline fraction indicates greater structural ordering within the carbon framework, reflecting the extent of graphitization achieved during pyrolysis [8].

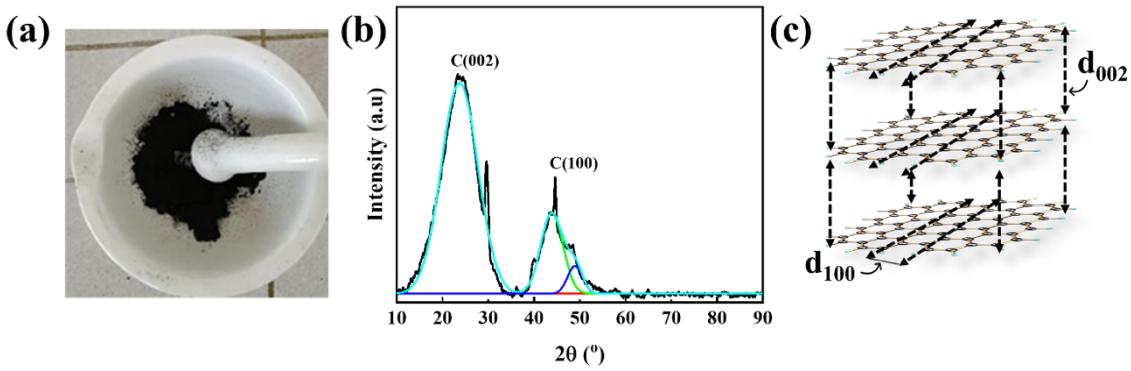

Figure 2. (a) Powder sample of BLG; (b) XRD pattern of BLG powder after baseline correction; (c) Schematic visualization of BLG layered structure.

The raw XRD data were processed using Origin software, with baseline correction applied to minimize background noise before calculating FWHM values, d-spacing, and crystallinity percentage. The calculated crystallographic parameters of the synthesized BLG are presented in Table 1 based on the XRD analysis.

The XRD analysis reveals two characteristic diffraction peaks of BLG at 2θ = 23.71° for the (002) plane and 2θ = 44.54° for the (100) plane. The (002) reflection corresponds to the stacking of graphene layers along the c-axis, which is directly related to the interlayer spacing (d-spacing). The measured d-spacing of 3.749 Å for the (002) peak is slightly larger than that of pristine graphite (≈ 3.35 Å), suggesting partial exfoliation, turbostratic disorder, or the presence of heteroatoms/defects that expand the interlayer distance.

The (100) reflection, with a d-spacing of 4.065 Å, is associated with in-plane periodicity of

the carbon lattice along the a-axis. This value indicates a certain degree of disorder in the basal plane, likely due to defects, vacancies, or heteroatom doping, which can disrupt the ideal sp^2 bonding network.

TABLE I. Calculated crystallographic parameters of BLG obtained from XRD analysis, including diffraction angle (2θ), Bragg angle (θ), interlayer spacing (d-spacing), full width at half maximum (FWHM), crystallite size (D), and crystallinity percentage.

Peaks	2θ (°)	θ (°)	d-spacing (Å)	FWHM(°)	Crystalite Size, D (nm)	Cristalinity (%)
(002)	23.71	12.005	3.749	7.811	0.995	46.80
(100)	44.54	22.27	4.065	5.195	1.415	

The crystallite size (D), calculated via the Scherrer equation, is relatively small (0.995 nm for (002) and 1.415 nm for (100)), indicating a nanoscale domain structure with significant edge effects. Such small crystallites typically enhance surface reactivity, which is beneficial for electrochemical applications but also signifies reduced long-range order.

The crystallinity percentage of ~46.80% suggests that the material has a mixed phase of crystalline and amorphous carbon. This moderate crystallinity reflects a balance between graphitic domains (providing good electrical conductivity) and amorphous regions (enhancing ion accessibility). From a chemical standpoint, the presence of defects and expanded interlayer spacing could facilitate ion intercalation/de-intercalation, making this BLG material potentially advantageous for battery anode or supercapacitor applications [11].

3.2. FTIR Study

FTIR spectroscopy was employed to identify the surface functional groups on the carbonaceous material and elucidate structural changes occurring during pyrolysis. FTIR spectra were collected 649.893 – 4000.6 cm^{-1}. The spectrum exhibited characteristic absorption bands corresponding to oxygen-containing functionalities,

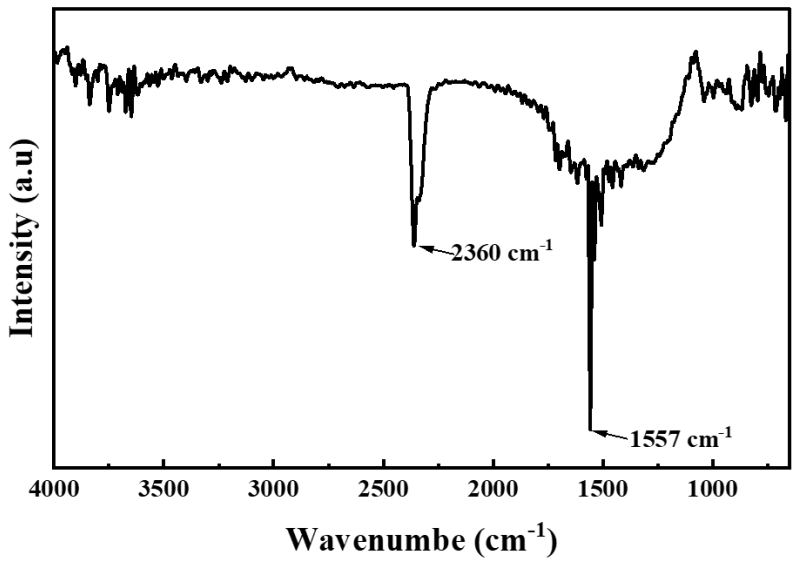

Figure 3. FTIR spectrum of BLG (649.893–4000.6 cm^{-1}), showing sp^2 C=C at 1557 cm^{-1} and CO_2 at 2360 cm^{-1}.

As shown in Figure 3. The FTIR spectrum of the synthesized carbon material exhibits two prominent absorption bands at approximately 2360 cm^{-1} and 1557 cm^{-1}. The sharp feature at 2360 cm^{-1} is attributed to the asymmetric stretching of atmospheric CO_2, which commonly appears as a background artifact during measurement rather than a material-specific functional group. In contrast, the intense band at 1557 cm^{-1} corresponds to the skeletal C=C stretching vibration of sp^2-hybridized

carbon within aromatic domains, indicating the development of graphitic structures. The absence of characteristic O–H stretching (~3400 cm^{-1}) and C=O stretching (~1720 cm^{-1}) suggests an effective removal of oxygen-containing functionalities during pyrolysis, consistent with the expected deoxygenation promoted by the activated carbon additive [8]. A weak signal in the region of 1100–1000 cm^{-1} may indicate residual C–O stretching from ether or epoxy groups, which can enhance surface wettability and facilitate electrolyte access without significantly compromising electrical conductivity [12]. These observations confirm that the thermal treatment strategy successfully produced a graphene-like structure with a low concentration of oxygen functionalities. This feature is highly desirable for improving electron transport and maintaining defect sites that are beneficial for electrochemical applications.

3.3. Scanning Electron Microscope Study

Figure 4 presents the SEM micrograph of BLG powder at 100.000× magnification, revealing a smooth layered morphology characteristic of stacked graphene sheets. The observed surface texture indicates well-developed planar structures with occasional wrinkles, typical for BLG materials synthesized via carbonization and exfoliation routes. The relatively continuous layers with minimal agglomeration suggest effective separation between graphene domains, promoting high surface area accessibility for electrolyte penetration.

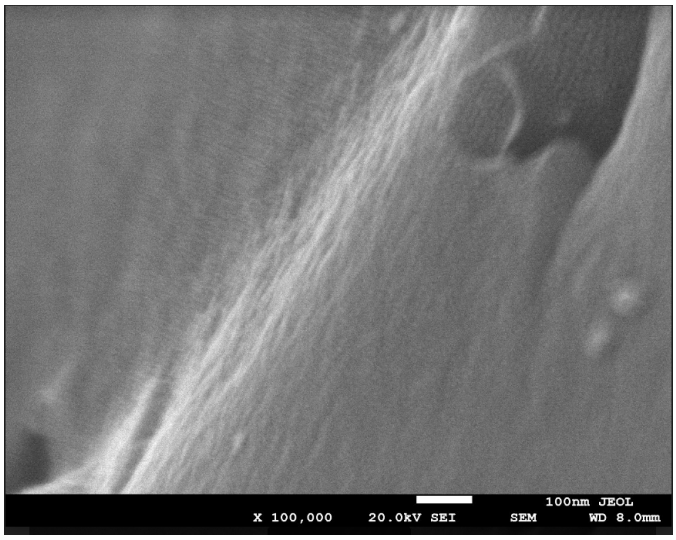

Figure 4. SEM image of BLG at 100,000×, showing layered and wrinkled nanosheets.

This structural feature is consistent with the increased electrical conductivity at higher voltages (Table 2, Figure 5a), as the interconnected graphene layers facilitate efficient charge transport pathways. Moreover, the wrinkle formations may serve as additional active sites for ion adsorption, contributing to the enhanced energy density values observed at 1.5 V (Table 3, Figure 2b). Therefore, the SEM evidence supports the electrochemical data, indicating that the optimized morphology of BLG enables a favorable balance between electrical conductivity and electrochemical storage performance.

3.4. Conductivity Measurement

The electrical conductivity of BLG was evaluated under various applied voltages (0.5, 1.0, and 1.5 V) over a 60-minute measurement period, as summarized in Table 2. The results indicate a clear dependence of conductivity on both the applied voltage and the measurement time. The electrochemical performance of BLG was comprehensively evaluated through electrical conductivity, power density, and energy density measurements under different applied voltages (0.5, 1.0, and 1.5 V). As shown in Table 2 and Figure 5(a), the electrical conductivity exhibited a clear positive correlation with the applied voltage, reaching 368.67 $\mu S \cdot cm^{-2}$ at 1.5 V after 60 minutes. This enhancement can be attributed to the improved charge carrier mobility and interfacial contact within the BLG network at higher driving potentials. Moreover, a slight time-dependent increase in conductivity suggests gradual electrolyte infiltration and stabilization of conductive pathways within

the electrode structure.

TABLE II. Electrical Conductivity (μS.cm^{-2}) of BLG.

Voltage (Volt)	Electrical conductivity (μS.cm^{-2}) of BLG					
	10 Min.	20 Min.	30 Min.	40 Min.	50 Min.	60 Min.
0	118.5	108.63	128.38	118.50	138.25	148.13
1.0	286.38	286.38	301.19	306.13	311.07	320.94
1.5	355.50	362.09	362.09	365.38	365.38	368.67

TABLE III. Power Density vs Energy Density of BLG.

Time (Minutes)	Power Density vs Energy Density of BLG					
	0.5 Volt		1.0 Volt		1.5 Volt	
	Power Density (W.Kg^{-1})	Energy Density (Wh.Kg^{-1})	Power Density (W.Kg^{-1})	Energy Density (Wh.Kg^{-1})	Power Density (W.Kg^{-1})	Energy Density (Wh.Kg^{-1})
10	0.24	2.40	2.32	23.2	6.68	64.8
20	0.22	4.20	2.32	46.2	6.6	132.0
30	0.26	7.80	2.44	73.2	6.6	198.0
40	0.24	9.60	2.48	99.2	6.66	266.4
50	0.28	14.0	2.52	126.0	6.66	333.0
60	0.30	18.0	2.60	156.0	6.72	403.2

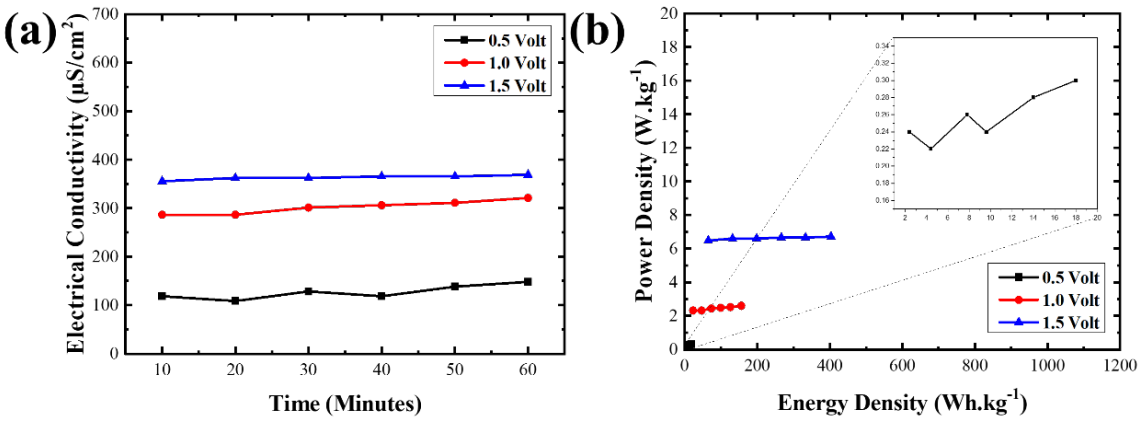

Figure 5. (a) Electrical conductivity (μS.cm^{-2}) of BLG; (b) Power density vs. energy density of BlG.

The corresponding power density and energy density values, presented in Table 3 and Figure 5(b), follow the expected Ragone plot behavior, where an increased applied voltage significantly elevates the energy density. In contrast, the power density remains relatively constant for each voltage condition. At 1.5 V, the BLG sample achieved the highest energy density of 403.2 Wh·kg^{-1} at a moderate power density of 6.72 W·kg^{-1} after 60 minutes, demonstrating its potential for high-energy storage applications. In contrast, the 0.5 V condition produced lower energy densities but gradually increased power density over time, indicating improved charge transport efficiency during prolonged cycling. These findings collectively reveal that BLG benefits from enhanced electrical conductivity at higher voltages and maintains a favorable balance between energy and power outputs. It is important to note that the energy and power density values presented here were derived from

conductivity-based measurements and serve as indicative parameters. Therefore, they should not be directly compared with literature values obtained from electrochemical cell testing of supercapacitors or batteries, but rather provide a preliminary insight into the charge transport and storage potential of BLG.

3.5. Antimicrobial Analysis

To further assess the potential antimicrobial properties of the prepared materials, the inhibition zone diameter, minimum inhibitory concentration (MIC), and minimum bactericidal concentration (MBC) were determined for both raw candlenut shell and its graphene nanosheet (BLG) derivative, as summarized in Table 4.

TABLE IV. Antibacterial activity of candlenut shell and BLG from candlenut shell based on inhibition zone diameter, MIC, and MBC

Samples	Inhibition Zone Diameter (mm)	MIC	MBC
Candlenut shell	0	-	-
BLG	10.76 ± 0.23	+	+

The antibacterial assay results in Table 4 clearly demonstrate the functional transformation achieved by synthesizing BLG from candlenut shell biomass. The pristine candlenut shell exhibited no measurable antibacterial activity, with a zero inhibition zone diameter and negative MIC/MBC values, indicating that the material lacks active sites or reactive functionalities necessary to inhibit bacterial growth in its raw form. In contrast, BLG derived from the same biomass showed a pronounced inhibition zone of 10.76 ± 0.23 mm and positive MIC and MBC values, signifying both inhibitory and bactericidal effects.

The improved antibacterial activity can be directly linked to the morphological and electronic changes observed in the material. SEM imaging (Figure 4) revealed a wrinkled sheet-like structure with abundant edges and defects, characteristic of exfoliated graphene, which enhances the interaction with bacterial membranes. Electrical conductivity measurements (Figure 5a) further indicated that BLG exhibits high charge transport capability due to restoring the sp^2 carbon network, facilitating electron transfer processes that can contribute to oxidative stress in bacterial cells.

The antibacterial activity of BLG can be further contextualized by comparing its performance with reported values from antibiotics and other graphene-based nanomaterials. The inhibition zone of BLG against *Salmonella typhimurium* (10.76 ± 0.23 mm) is lower than that of standard antibiotics such as ciprofloxacin, which typically produces inhibition zones greater than 20 mm [13]. However, the antibacterial effect of BLG is comparable to or higher than several biomass-derived graphene materials, which generally exhibit inhibition zones in the range of 7–12 mm [14]. In addition, the positive MIC and MBC responses observed for BLG demonstrate both inhibitory and bactericidal activity, highlighting its potential as a carbon-based nanomaterial with multifunctional properties. Although not as strong as conventional antibiotics, the antibacterial performance of BLG is significant considering its sustainable synthesis route from candlenut shell biomass and its dual role as both a conductive and antimicrobial material.

Meanwhile, the Power Density vs. Energy Density profile (Figure 5b) confirmed that BLG possesses an optimal balance between high energy storage capacity and rapid charge–discharge capability. Although this metric is primarily used to evaluate electrochemical performance, the high surface activity and defect-rich architecture responsible for such energy–power characteristics also enhance antibacterial efficiency by providing more reactive contact sites and enabling efficient charge transfer interactions with microbial membranes.

In fundamental terms, the antibacterial mechanism of BLG involves a synergy between mechanical damage from nanosheet edges, oxidative stress via reactive oxygen species (ROS) formation, and electron transfer–induced metabolic disruption in bacterial cells [15]. Collectively, these findings establish that converting candlenut shell biomass into BLG yields superior electrochemical materials and results in multifunctional nanostructures with significant antibacterial potential, expanding their applicability to energy, environmental, and biomedical domains.

4. CONCLUSIONS

We developed a scalable pyrolysis method to synthesize biomass-derived graphene nanosheets (BLG) from candlenut shells, achieving defect-rich, low-oxygen sp^2 carbon structures with high conductivity and electrochemical performance. BLG reached 368.67 $\mu S \cdot cm^{-2}$ conductivity at 1.5 V, with stable power and high energy density, while exhibiting potent antibacterial activity against *Salmonella typhimurium*. These multifunctional properties position BLG as a sustainable nanomaterial platform for next-generation energy storage and antimicrobial applications.

Acknowledgement

The authors gratefully acknowledge Yosia Manik for his valuable assistance in data processing, Wenny Simbolon, and Ruth Siburian for their contributions to the experimental work.

References

[1] J. Alisa, A. Hutapea, Y. Gopas, O. Manik, S. Theo, and C. Lotebulu, "Comprehensive Review of Graphene Synthesis Techniques : Advancements, Challenges, and Future Directions Comprehensive Review of Graphene Synthesis Techniques : Advancements, Challenges, and," pp. 0–35, 2025, doi: 10.20944/preprints202507.1219.v1.

[2] N. Kumar, K. Setshedi, M. Masukume, and S. S. Ray, "Facile scalable synthesis of graphene oxide and reduced graphene oxide: comparative investigation of different reduction methods," *Carbon Lett.*, vol. 32, no. 4, pp. 1031–1046, 2022, doi: 10.1007/s42823-022-00335-9.

[3] Y. G. O. Manik, B. T. Goh, and R. Siburian, "Low-Cost Synthesis of Biochar-Like Graphene From Coconut Shells: Enhancing Conductivity for Electrochemical Applications," *Rasayan J. Chem.*, vol. 18, no. 1, pp. 318–324, 2025, doi: 10.31788/RJC.2025.1819132.

[4] A. L. Olatomiwa, T. Adam, S. C. B. Gopinath, S. Y. Kolawole, O. H. Olayinka, and U. Hashim, "Graphene synthesis, fabrication, characterization based on bottom-up and top-down approaches: An overview," *J. Semicond.*, vol. 43, no. 6, p. 61101, 2022, doi: 10.1088/1674-4926/43/6/061101.

[5] E. Pasaribu, R. Siburian, and M. Supeno, "Production of Graphene By Coconut Shell As an Electrode Primary Battery Cell," *Elkawnie*, vol. 9, no. 1, p. 37, 2023, doi: 10.22373/ekw.v9i1.14880.

[6] R. Siburian *et al.*, "Converting Candlenut Shell Waste into Graphene for Electrode Applications," *Processes*, vol. 12, no. 8, 2024, doi: 10.3390/pr12081544.

[7] Y. Wibisono *et al.*, "Preparation of Activated Carbon from Local Biowaste as Fillers for Mixed Matrix Membranes," vol. 2, pp. 517–528, 2023, doi: 10.2991/978-94-6463-140-1_52.

[8] Y. G. O. Manik, B. T. Goh, R. Siburian, and Y. Alias, "Synthesis of Graphene Nanosheets from Coconut and Candlenut Shells: Large-Scale Production and Application in Fe Ion Adsorption and Electrochemical Properties," *ACS Omega*, vol. 10, no. 4, pp. 3338–3350, Jan. 2025, doi: 10.1021/acsomega.4c05745.

[9] K. Tarigan *et al.*, "Synthesis and Characterization of Coconut-Derived Graphene Nano Sheet (GNS) and Its Properties in Nickel/GNS and Zinc/GNS Hybrid Electrodes," *Processes*, vol. 12, no. 1943, 2024, doi: https://doi.org/10.3390/pr12091943.

[10] H. F. Hamdan, E. E. R. Ross, M. T. M. Jalil, M. A. Hashim, and M. F. Z. R. Yahya, "Antibiofilm Efficacy and Mode of Action of Etlingera elatior Extracts Against Staphylococcus aureus," *Malaysian Appl. Biol.*, vol. 53, no. 1, pp. 27–34, 2024, doi: 10.55230/mabjournal.v53i1.2808.

[11] J. Wang *et al.*, "Balancing Graphitic Nanodomains and Heteroatom Doping in Hard Carbons Toward High Capacity and Durable Potassium-Ion Battery Anodes," *Adv. Funct. Mater.*, vol. 34, no. 51, p. 2409937, Dec. 2024, doi: https://doi.org/10.1002/adfm.202409937.

[12] K. Tarigan, R. Siburian, E. A. M. Sitorus, F. J. Purba, and Y. G. O. Manik, "Fabrication and Optimization of Primary Batteries Using Ni/Graphene Nanosheet Electrodes," *Sci. Technol. Indones.*, vol. 9, pp. 413–426, Apr. 2024, doi: 10.26554/sti.2024.9.2.413-426.

[13] M. F. Z. R. Yahya, Z. Alias, and S. A. Karsani, "Subtractive Protein Profiling of Salmonella typhimurium Biofilm Treated with DMSO," *Protein J.*, vol. 36, no. 4, pp. 286–298, 2017, doi: 10.1007/s10930-017-9719-9.

[14] S. S. Nasker, P. M. Ajayan, and S. Nayak, "Emerging Trends and Future Direction of Graphene Family of Materials as Potential Antimicrobials: A Critical Review," *ACS Mater. Lett.*, vol. 5, no. 3, pp. 673–693, Mar. 2023, doi: 10.1021/acsmaterialslett.2c01116.

[15] Y. Chen, S. Pandit, S. Rahimi, and I. Mijakovic, "'Graphene nanospikes exert bactericidal effect through mechanical damage and oxidative stress,'" *Carbon N. Y.*, vol. 218, no. December 2023, 2024, doi: 10.1016/j.carbon.2023.118740.